Tosun G., Bakker A. (1997) A Study of Macrosegregation in Low-Density Polyethylene Autoclave Reactors by Computational Fluid Dynamic Modeling, Ind. Eng. Chem. Res., Vol. 36, No. 2, page 296-305.

A Study of Macrosegregation in Low-Density Polyethylene Autoclave Reactors by Computational Fluid Dynamic Modeling

Güray Tosun*

DuPont, Central Research & Development, Wilmington, Delaware 19880-0304

André Bakker

Chemineer, Inc., Dayton, Ohio 45401-1123

Flow and reaction in a typical commercial scale autoclave LDPE reactor were modeled by a three-dimensional computational fluid dynamic (CFD) $k-\epsilon$ model in order to shed light on the macrosegregation effects that can occur in these reactors. It is shown that the CFD model predicts significant differences from CSTR behavior. Results are discussed in terms of the effects of macro- and microscale inhomogeneities of concentration and temperature on free radical polymerization kinetics. The observed nonidealities in terms of minima in the initiator consumption curves and multiple steady states are explained on the basis of competing turbulent transport and chemical kinetics. Microsegregation effects are shown to be negligible in comparison to macrosegregation effects. Given the fact that the CFD model is based on reactive scalar and energy balances without adjusted parameters in the three-dimensional flow field of the entire reactor, it is tentatively concluded that commercial-scale LDPE vessel reactors can have significant macrosegregation effects beyond a certain steady-state adiabatic operating temperature that is specific to the initiator being used.

Introduction

Polyethylene (PE) resins, produced commercially for over 50 years, have become a global business. In 1992, world production of PE was 33 million metric tons. On the basis of world consumption, PE represented 70% of polyolefins and 44% of all thermoplastic resins, while consuming about half of world ethylene output. As of 1992, low-density polyethylene (LDPE) accounted for 40% of the world PE capacity (Stanford Research Institute, 1995). LDPE is produced in adiabatic autoclaves or tubular reactors by free radical polymerization of ethylene at high temperature (140−300 °C) and high pressure (100−3500 atm). Autoclaves account for about half of the total LDPE production. The autoclave reactors are operated at low conversions for safety reasons. Relatively high feed flow rates and short residence times that are typical for these reactors often result in a feed jet with composition and temperature significantly different from the rest of the reactor vessel. These macroscale inhomogeneities due to the presence of the feed jet can create a significant macrosegregation effect on the performance of these reactors as compared to the predictions from a continuously stirred tank reactor (CSTR) model. There have been a number of mathematical models, published over the last two decades, that addressed the "mixing" issue in the vessel reactors. A review of these models is given by Kipparissides *et al.* (1993). Of particular industrial interest is the relationship between the initiator content of the feed and the steady-state operating temperature of an adiabatic vessel reactor since this is the main relationship that governs the steady-state operating conditions of the reactor including the presence of multiple steady states. The consequent relationship between the initiator consumption per unit mass of polymer and the operating temperature is also of high industrial significance since initiator costs are an important fraction of the variable costs. The latter relationship has been investigated experimentally in laboratory reactors by Luft and Bitsch (1977), van der Molen *et al.* (1972, 1982), and Mercx *et al.* (1972). These workers showed that the consumption versus temperature curve for a given initiator displays a characteristic minimum as the operating temperature is increased. A number of workers attempted to model this behavior mathematically. Mercx *et al.* (1972) predicted the observed minimum by a model consisting of a plug flow reactor with recycle. Marini and Georgakis (1984a,b) used a compartmental zone model which represented the feed jet as two small CSTRs of equal volume in series with the rest of the vessel also represented as a CSTR with recycle to the small CSTRs. The volume of the small CSTRs and the recycle flow that each one received were the model parameters. These parameters were estimated by the authors for the laboratory scale reactor of the study by van der Molen *et al.* (1982) for a jet of assumed size and shape through mass and momentum balances. Good agreement between model predictions and experimental data was found. Zwietering (1984) presented a "plume model" where the plume of the feed jet would exponentially grow by mixing with the bulk until concentrations inside the plume become the same as those in the bulk. With proper choice of the parameter p, the time constant for the growth of the plume, the model would qualitatively predict the observed minimum in the consumption curve. In what is essentially a zone model, Smit (1992) fixed the size of the jet ("flame") in terms of the kinematic viscosity and turbulent energy dissipation rate and qualitatively predicted the minimum by a model similar to the engulfment model of Baldyga and Bourne (1984). The size of the flame which is the adjustable parameter of Smit's model had a significant effect on the location of the minimum. A computational

* Author to whom correspondence should be addressed.

S0888-5885(96)00374-0 CCC: $14.00

fluid dynamic model of LDPE autoclaves addressing macrosegregation effects has not been found in the literature.

In the present study, predictions of a three-dimensional computational fluid dynamic (CFD) model for a typical commercial scale autoclave reactor with premixed feed (monomer and initiator) are compared with the predictions of a model for an adiabatic CSTR with premixed feed. The CFD model consisted of sequential solution of the flow followed by solution of the passive (reactive) scalar and energy balances for free radical homopolymerization in a fixed flow field that was assumed unaffected by the reactive scalars and temperature. Numerical results by the two models have been used to construct plots of feed initiator concentration and initiator consumption versus adiabatic operating temperature. Two different initiators were investigated in order to distinguish the effects of initiator kinetics on the relationships of interest.

There appears to be no data in the literature relating feed initiator concentration to steady-state operating temperature in commercial scale autoclave reactors. Moreover, published experimental studies of initiator consumption in laboratory scale reactors (van der Molen *et al.*, 1972, 1981; Luft and Bitsch, 1977) do not include details of the reactors that were used in these studies.

General Assumptions

Both the CFD and the CSTR models were based on a single set of assumptions regarding kinetics, thermodynamics, and physical properties in order to maintain a consistent basis of comparison. Kinetics were limited to initiation, propagation, and termination by combination with gel effect. Transfer and scission reactions that mainly affect the molecular weight distribution were not included since molecular weight distribution does not influence the relationships of interest. Since conversion in commercial reactors is under 20%, it was assumed that physical properties of the reacting medium, i.e., density, heat capacity, viscosity, and thermal conductivity, do not vary throughout the reactor. As it will be discussed later, the CFD flow solution was relatively insensitive to the relevant physical properties density, viscosity, and molecular diffusion. Therefore, composition-dependent physical properties would have resulted in slightly very different temperature and concentration values in the reactive scalars modeling stage of the CFD solution (see below) while greatly increasing the computation times which were considerable (see discussion of computation times below). Thus, physical properties corresponding to the outlet temperature of the reactor were used as constant throughout the grid in each computation. It was assumed that heat of reaction by propagation (8.95×10^7 J/(kg mol)) was the only chemical energy source that contributed to the enthalpy balances. Heat effect of the initiation and termination steps were neglected.

Kinetic Model

The lumped treatment of free radical chain addition polymerization (Ray, 1972) with initiation, propagation, and termination by combination was used with the inclusion of a gel effect function g_t for diffusion-controlled termination. The basic reactions and the kinetic rate equations that constituted the source terms for the individual species in each model were

Table 1. Reaction Kinetic Data

k (kg mol)/(m^3 s)	A	E_a J/(kg mol)	$V_a \times 10^2$ J/(kg mol Pa)	f
k_p	1.88×10^7	3.433×10^7	−11.296	
k_{tc0}	1.60×10^9	0.460×10^7	6.628	
k_d (initiator A)	3.49×10^{16}	14.269×10^7	0.251	0.8
k_d (initiator B)	1.35×10^{14}	11.698×10^7	0.251	0.8

initiator decomposition:

$$I \xrightarrow{k_d} 2R_1^{\bullet} \tag{1a}$$

$$S_I = -k_d I \tag{1b}$$

propagation:

$$M + R_n^{\bullet} \xrightarrow{k_p} R_{n+1}^{\bullet} \tag{2a}$$

which, when summed over all radicals, leads to

$$S_M = -k_p MR \tag{2b}$$

termination:

$$R_n^{\bullet} + R_m^{\bullet} \xrightarrow{k_{tc}} P_{n+m} \tag{3a}$$

which, when summed over all radicals, leads to

$$S_R = 2fk_d I - k_{tc} R^2 \tag{3b}$$

where $R_n^{\bullet}$ is the growing radical, R is the total radical concentration, and f is the initiator efficiency factor. Reaction rate constants were of the form

$$k = A \exp(-E_a/(RT) - (V_a P)/(RT)) \tag{4}$$

where V_a is the activation volume. The termination rate constant k_{tc} is the product of k_{tc0}, the rate constant at zero conversion, and g_t, the gel effect function that accounts for the decrease in the termination rate due to increasing conversion, hence reduced chain-end mobility. The gel effect function g_t was (Buback, 1990)

$$g_t = 1/(a\log_{10}(5.39x + 3.7x^{0.5})) + 1400k_p(1 - x)/k_{tc0} \tag{5}$$

where x is the monomer conversion.

The parameters of the rate constants used are given in Table 1. The initiators A and B were commercial initiators of peroxide type.

CFD Model

Modeling LDPE reactors with computational fluid dynamics is relatively new with few reports in the open literature (Torvik *et al.*, 1995). CFD affords the only means to model an asymmetric reactor in three dimensions with the ability to solve mass, momentum, and energy equations throughout the computational domain. We have used FLUENT version 4.2 to model flow and version 4.3 (Fluent, Inc., 1995) to model polymerization by passive scalars option in a typical industrial-scale reactor (Chan *et al.*, 1993) which had an *L/D* of about 4, a multiple-impeller agitator, a single feed jet introduced vertically at the top outside the perimeter of the

impeller blades, and an outlet tube on the bottom 180° from the inlet. A two-stage approach was followed, in order to reduce the computational complexity of the problem, whereby the steady-state flow solution was carried out first, followed by the solution of steady-state convection–diffusion equations for concentrations of initiator, monomer, and total radicals simultaneously with adiabatic enthalpy balances in the flow field that had been computed in the preceding stage. This was justified under the assumption that in full turbulence the effects of reaction in terms of physical property changes on the flow solution are negligibly small. The relative insensitivity of the flow solution to physical properties was established by performing preliminary flow solutions at constant physical properties that varied between runs more than the estimated local variations of physical properties due to local values of temperature and composition that were expected in the calculations with reaction. Hence, in order to minimize overall computation time and effort, flow solution at a single temperature was used for all the reaction work.

CFD Model of Flow. A three-dimensional asymmetric grid with 87 696 cells (58 × 24 × 63) was used for the reactor vessel. The impellers were modeled by prescribing experimental boundary conditions for the velocities, the turbulent kinetic energy, and the turbulent energy dissipation rate in the outflow of the impellers. The impeller boundary conditions were obtained from laser-Doppler velocimetry data by Wang *et al.* (1995). Wang's measurements were performed in a smaller vessel (0.3 m in diameter). The velocities were normalized by the impeller tip speed and then rescaled to the current reactor size and impeller speed. This method is described in more detail by Bakker and Van den Akker (1994). The boundary conditions were obtained using laser-doppler velocimetry by Wang *et al.* (1995). The $k-\epsilon$ model was used to model the turbulent Reynolds stresses. In FLUENT 4.2, the multigrid solver was used to solve the pressure equation and the standard Line-Gauss-Seidel (LGS) solver was used for the other quantities. A power law differencing scheme was used in the discretization.

When the scalar equations governing the polymerization reactions were solved, no special modeling of the impeller region was performed. Rather, the impeller region was considered a normal part of the flow domain, except for the prescribed boundary conditions in the outflow. Obviously, this may lead to an underprediction of the mixing intensity in the impeller region, but the effect on the overall predictions is expected to be small, since the impellers make up a relatively small part of the whole reactor.

CFD Model of Reaction in Turbulent Flow Field. The reactive species balances option of FLUENT which is designed to deal with chemically reacting species cannot be used for the lumped kinetic model of free radical addition polymerization due to the fact that in the lumped model the propagation reactions shown in eq 2a are summed for all radicals to yield

$$M + R \xrightarrow{k_p} R$$

where R is the total radical concentration. This pseudoreaction cannot be described in the reactive species balances option of FLUENT since reactive species R would have to be assigned a stoichiometric coefficient of +1 as a reactant and −1 as a product whereas only one coefficient per species is allowed. However, one can use the scalar balances option recently included in FLUENT (version 4.3) and treat I, M, and R as passive scalars with source terms given by eqs 1b–3b.

For the general case of the bimolecular reaction obeying the mass–action law

$$A + B \xrightarrow{k} C$$

occurring in a turbulent medium, the time-mean convection diffusion equation can be expressed as

$$\frac{\partial \bar{C}_A}{\partial t} + \nabla\cdot\bar{V}\bar{C}_A = \nabla\cdot(D\nabla\bar{C}_A - \overline{V'C_A'}) - k(\bar{C}_A\bar{C}_B + \overline{C_A'C_B'}) \quad (6)$$

where the term $\overline{V'C'_A}$ represents turbulent diffusion down the mean gradient created by correlated velocity and concentration fluctuations. With the usual mass and momentum transfer analogy based on the well-known turbulent viscosity closure of the $k-\epsilon$ model, this term is closed in terms of the turbulent diffusivity D_t defined analogously to the turbulent viscosity

$$\overline{V'C'_A} = -D_t\nabla\bar{C}_A \quad (7)$$

thus, eq 6 is transformed to

$$\frac{\partial \bar{C}_A}{\partial t} + \nabla\cdot\bar{V}\bar{C}_A = \nabla\cdot(D_{eff}\nabla\bar{C}_A) - k(\bar{C}_A\bar{C}_B + \overline{C_A'C_B'}) \quad (8)$$

where $D_{eff} = D + D_t$.

This closure still leaves the scalar covariance term $k\overline{C_A'C_B'}$ to be closed. This term describes the effect of concentration fluctuations on the local time-mean reaction rate (microsegregation, Hanks and Toor, 1995). This term is handled by different closures depending on the particular model being used (Frankel *et al.*, 1993).

In FLUENT (4.3) scalar balances applied to C_A can be expressed as

$$\frac{\partial \bar{C}_A}{\partial t} + \nabla\cdot\bar{V}\bar{C}_A = D_{eff}\nabla^2\bar{C}_A + S_A \quad (9)$$

where D_{eff} is the effective diffusivity and S_A is the source term for C_A, both of which can be defined by the user. Following the mass–momentum transfer analogy between D_t and μ_t of the $k-\epsilon$ model, D_{eff} has a default definition as

$$D_{eff} = D + 0.09k^2/\epsilon \quad (10)$$

The source term S_A is linearized as

$$S_A = \alpha + \beta\bar{C}_A \quad (11)$$

where α and β are constants specified by the user. For the example reaction above α and β would be defined as zero and $-k\bar{C}_B$, respectively. The important point about the scalar source term S_A in eq 11 is that it is defined in terms of the time-mean concentrations with no provisions for the scalar covariance term. Thus any closure to be introduced through user-defined routines of FLUENT (4.3) would have to be in terms of the time-mean concentrations of the reactive scalars involved.

Of the three reactions involved (eqs 1a–3a), initiator decomposition is first order for which the scalar covariance term is zero; i.e., microsegregation does not affect initiator decomposition. Thus, source terms including

the covariance terms for the three scalars and enthalpy that would satisfy eq 8 would be as follows

reactive scalars:

$$S_I = -k_d\bar{I} \tag{12}$$

$$S_M = -k_p(\bar{M}\bar{R} + \overline{M'R'}) \tag{13}$$

$$S_R = 2fk_d\bar{I} - k_{tc}(\bar{R}\bar{R} + \overline{R'R'}) \tag{14}$$

enthalpy:

$$S_h = -k_p(\bar{M}\bar{R} + \overline{M'R'})\Delta H \tag{15}$$

Note that the possible effect of the temperature fluctuations on the rate constants is not included in the above expressions. This question will be addressed in the discussion to follow.

Closure of Microsegregation Terms

In its treatment of the reactive species balances, FLUENT uses a semiempirical closure where the source term changes from time-mean reaction rate to eddy breakup rate calculated in terms of time-mean concentrations, turbulence quantities, and two adjustable constants. Although it was out of the question to use this option since the reactive species option was not available for the problem at hand, it would be possible to introduce a similar closure into the user-defined subroutine of FLUENT for the scalar source terms. However, no exact closure of proven accuracy exists for the complex kinetics of the lumped free radical kinetics described above. Thus, the probability of introducing unnecessary error is great. Instead, a conservative analysis of the relative rates of local micromixing and reaction was performed in order to judge the relative importance of the covariance terms, as will be discussed below.

For reactions of order higher than one, microsegregation affects the reaction rate, while for multiple reactions, it affects product distribution. Thus, in a detailed kinetic model of free radical homopolymerization, microsegregation can conceivably affect molecular weight distribution (MWD). However with the lumped kinetic model, where the total radical concentration is defined as a single scalar R, calculation of the individual radical chain concentrations and hence any microsegregation effects of the radical concentrations on MWD is neither possible nor, in the present work, sought for. Therefore, with the kinetic model employed in the present study, the only microsegregation effects to consider are those due to the covariance terms in eqs 13−15.

Whether there can be appreciable contributions from the covariance terms in eqs 13−15 can be judged by comparing the time scale within which diffusion homogenizes local fluctuations of concentration and the time scale for the reaction in question. Baldyga and Bourne (1984) developed an expression for diffusion time under the stretching and deforming effects of turbulent strain (Tennekes and Lumley, 1987) as

$$t_{DS} \approx (\nu/\epsilon)^{1/2}\,\mathrm{arcsin}(0.1Sc) \tag{16}$$

where ν is the kinematic viscosity, ϵ is the turbulent energy dissipation rate, and Sc is the Schmidt number (ν/D). Thus, one can define Da_2 the local Damköhler number based on diffusion time as t_{DS}/t_{rxn}. The value of Da_2 for termination and propagation would then be given by $Da_{2R} = t_{DS}/t_c$ and $Da_{2M} = t_{DS}/t_p$ where $t_c = 1/(k_{tc}R)$ and $t_p = \ln 2/(k_pR)$ (since propagation is effectively first order). The value of t_{DS} can be easily calculated from the results of the CFD flow solution. When the numerical value of Da_2 is less than unity (1.0), molecular diffusion would remove the small scale concentration inhomogeneities created by the fluctuations due to turbulence before reaction could occur to an appreciable extent. Then the concentrations would be effectively at their time-mean values relative to reaction time scales. The greatest fluctuations of radical concentration are expected to occur in the jet where the greatest gradients of concentration are likely to be found. Therefore, the most conservative estimate of Da_2 would correspond to the highest expected value of temperature (based on expected conversion) and the total radical concentration in the jet. These estimates were carried out for both initiators, and the maximum expected values of Da_{2R} and Da_{2M} were found to be less than unity (ca. 0.8 and 4.0×10^{-4}). It was therefore concluded that the covariance terms in the source equations (eqs 13−15) could be safely dropped to yield

$$S_M = -k_p\bar{M}\bar{R} \tag{17}$$

$$S_R = 2fk_d\bar{I} - k_{tc}\bar{R}\bar{R} \tag{18}$$

$$S_h = -k_p\bar{M}\bar{R}\Delta H \tag{19}$$

The above equations constitute the so called "product of the means" (POM) closure which is well justified for cases where Da_2 is less than one. As it will be discussed later, following the CFD calculations a much more detailed analysis of this closure based on calculations of the local values of Da_{2R} and Da_{2M} from the CFD results was carried out, and the above assumption was shown to be well born out by the results.

As for the temperature fluctuations, one can derive the temperature equivalent of eq 16, for the time scale for thermal diffusion to remove local temperature fluctuations. The new equation would have the Prandtl number Pr ($=\nu/\gamma$) instead of the Schmidt number inside the parentheses (see eq 16). Since thermal diffusivity γ is about 150 times the molecular diffusivity for ethylene at the conditions of the computations, the temperature equivalents of Da_2 were found to be much less than the estimates found for the maximum possible expected values of Da_2 for molecular diffusion. Thus, temperature fluctuations were not considered.

Convergence Criteria. Convection−diffusion equations for the concentration scalars and enthalpy were solved simultaneously in a fixed flow field (unaffected by reactive scalars or temperature) by the Line-Gauss-Seidel solver of FLUENT 4.3. An SGI Challenge XL machine with six R4400 200MHz processors (OS: 32 bit Irix 5.3) and a main memory of 768 MB was used on a time-sharing basis. For convergence, in addition to FLUENT's convergence criteria of relative residuals of the discretized equations decreasing to user-defined tolerances, an additional convergence condition was imposed through user-defined subroutines that required the temperature rise from input-to-output to be within a specified tolerance of the adiabatic temperature rise computed from the mean outlet conversion. Typical run times are given in the discussion section.

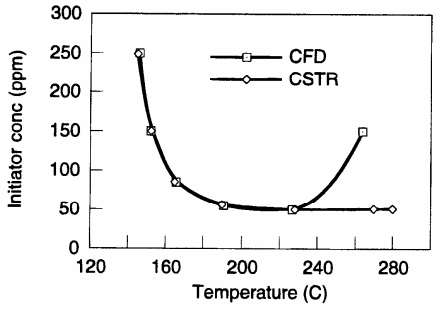

Figure 1. Feed initiator concentration versus adiabatic steady-state outlet temperature for initiator A.

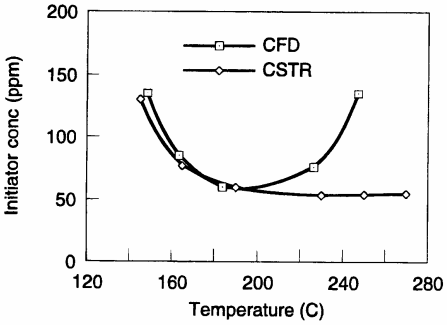

Figure 2. Feed initiator concentration versus adiabatic steady-state outlet temperature for initiator B.

CSTR Model

Steady-state mass balances for initiator, monomer, and total radicals and the adiabatic enthalpy balance given below were solved subject to the general assumptions discussed above.

$$0 = QI_0 - QI - k_dIV \tag{20}$$

$$0 = QM_0 - QM - k_pMRV \tag{21}$$

$$0 = -QR + 2fk_dIV - k_{tc}R^2V \tag{22}$$

$$0 = \rho C_pQ(T_0 - T) + (-\Delta H)k_pMRV \tag{23}$$

Discussion of Results

Figures 1 and 2 show the results for feed initiator concentration against steady-state outlet temperature for initiators A and B, respectively. In all cases the feed consisted of premixed initiator and ethylene at 40 °C. The symbols in the figures represent computed results for different cases with each model. The smooth curves through symbols are for identification purposes and not necessarily for interpolation. The relatively few number of runs with the CFD model for each initiator (six and five, respectively) is due to the time-intensive nature of the runs which on average took about 20 h of computation for successful convergence. In Figure 1 (initiator A), the CFD curve follows the CSTR curve up to about 230 °C after which it rises appreciably above the latter at about 265 °C. Figure 2 (initiator B), which has somewhat faster decomposition kinetics over the temperature range of interest (e.g., $t_{1/2}$ at 165 °C is 0.6 s for B versus 2.7 s for A), exhibits a similar comparison of the two models with a minimum in the CFD curve at

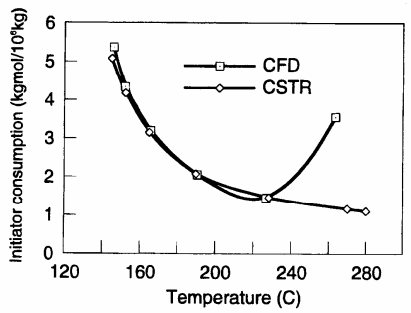

Figure 3. Specific initiator consumption versus adiabatic steady-state outlet temperature for initiator A.

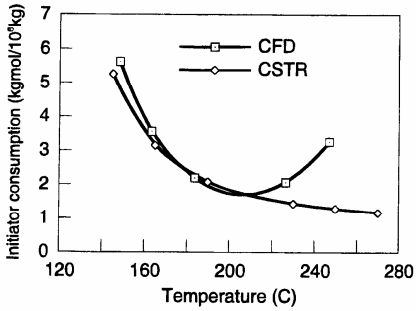

Figure 4. Specific initiator consumption versus adiabatic steady-state outlet temperature for initiator B.

about 190 °C after which the latter rises greatly above the CSTR curve. It may be concluded from Figures 1 and 2 that the CFD model exhibits steady-state multiplicity evidenced by a minimum in the initiator concentration versus temperature curve at a temperature specific to the particular initiator. The onset of multiplicity is earlier for the faster initiator. The CSTR model does not exhibit steady-state multiplicity over the range of temperatures of interest for either initiator. In both Figures 1 and 2, if taken to high enough initiator concentrations, the rise on the left side of both CFD and CSTR curves would exhibit a peak with a very steep left flank corresponding to light off from the cold feed conditions. Similarly, if taken to high enough temperatures the flat right-hand side of the CSTR curve would probably exhibit an upturn corresponding a second steady state. Thus, the rise on the left-hand side of both model curves in Figures 1 and 2 probably corresponds to a metastable steady state. However, commercial LDPE reactors are often successfully operated around a metastable point by means of closed-loop control of the inlet initiator concentration.

Figures 3 and 4 show specific initiator consumption ((kg mol)/10^6 kg polymer) against steady-state outlet temperature for initiators A and B, respectively. The same trends as in concentration versus temperature curves of Figures 1 and 2 are observed in Figures 3 and 4. The minima exhibited in the CFD curves of Figures 3 and 4 are significant not only because they confirm experimental findings in laboratory-scale vessels discussed earlier but also because the shape of these curves can help explain the trends in the CFD results as will be seen below.

Prior to attempting an interpretation of the specific results shown in Figures 1–4, it is instructive to consider the potential effects of macrosegregation on the

Table 2. Summary of Results for Selected CFD Runs with Initiator A

feed init (ppm)	value at	temp (°C)	$I \times 10^4$	M	$R \times 10^5$	R/R_{out}	Da_{1I}	Da_{1R}	KCL $\times 10^{-3}$	KCL/KCL$_{out}$	IC/IC$_{out}$	Da_{2R}	$Da_{2M} \times 10^{-3}$
250	jet	131	6.1	20.0	0.028	0.2	0.0003	0.3	4.6	1.0	1.0	0.008	0.0008
	outlet	146	4.1	18.7	0.15	1.0			4.4	1.0	1.0	0.05	0.02
50	jet	217	0.33	17.4	0.057	4.1	0.6	0.4	16.3	0.2	5.8	0.009	0.007
	outlet	227	5.5×10^{-6}	15.9	0.014	1.0			95.3	1.0	1.0	0.007	0.009
150	jet	236	1.33	17.5	1.43	255	2.3	19.4	0.4	0.002	585	0.5	0.23
	outlet	264	0.00	14.7	0.0056	1.0			234	1.0	1.0	0.005	0.006

performance of an LDPE vessel reactor. Generally speaking macrosegregation, i.e., concentration gradients on macroscopic scales, can create high local mean concentrations which, when combined with high enough temperatures, can produce high local reaction rates and great departures from CSTR predictions particularly where there are competing reaction paths. In the particular case of interest here, reactions 1a, 2a, and 3a in effect constitute a network made up of a first-order reaction (initiator decomposition) followed by two parallel reactions: propagation which is a pseudo-first-order reaction due to lumping and termination which is a pseudo-unimolecular second-order reaction. In general, time scales of these reactions, i.e., t_d for initiator decomposition, t_c for radical termination by combination, and t_p for propagation relative to the time scale of turbulent diffusion, which is k/ϵ, would determine whether there can be macrosegregation and the extent to which macrosegregation would affect steady-state reactor operation. Thus, the first Damköhler number, the ratio of the turbulent diffusion time scale to the reaction time scale, is the critical dimensionless number to consider. One can examine the first Damköhler number for initiation and termination in order to understand the results of the CFD model calculations. If Da_{1I} ($=k/\epsilon t_d$) is small, obviously nothing will happen in the jet since turbulent diffusion would disperse the initiator before it can decompose. If Da_{1I} is greater than 1.0, on the other hand, then the value of Da_{1R} ($=k/\epsilon t_c$) and Da_{1M} ($=k/\epsilon t_p$) will determine whether the radicals will react in the jet (either to terminate prematurely or to propagate) or whether they will be dispersed by turbulent diffusion into the reactor bulk to react at the reaction rates that exist in the bulk. Since by definition $t_c = 1/k_{tc}R$ and $t_p = \ln 2/(k_pR)$ (since propagation is effectively first order) and k_{tc} is much higher than k_p over the temperature range of interest, one needs only to consider Da_{1R} at this stage. Thus, any factor which increases Da_{1I} and Da_{1R} together above unity will contribute to premature reaction in the jet. On the other hand, the relative reaction rates of propagation and termination will determine the relative extent to which the radicals take part in propagation, which generates heat to sustain adiabatic temperatures, as opposed to the extent to which they (radicals) take part in termination which consumes radicals without generating heat. Thus, any factor which lowers the ratio of propagation rate to termination rate, i.e., $k_pM/k_{tc}R$, will cause an increase in the amount of initiator required to maintain a specific adiabatic temperature. Furthermore, a lowering of the ratio $k_pM/k_{tc}R$ will indicate premature termination of the radicals and hence inefficient utilization of the initiator. Therefore, by considering local values of Da_{1I} and Da_{1R} and the ratio $k_pM/k_{tc}R$, one can explain the trends seen in Figures 1–4.

In the following subsections, the computed trends exhibited by the CFD model results for each initiator will be qualitatively explained in terms of the effects macrosegregation on reaction kinetics. Microsegregation closure discussed above will be reexamined subsequently with the aid of the computed results.

Initiator A. Table 2 summarizes data relevant to macrosegregation effects for three selected CFD model runs for initiator A. Presented in Table 2 are jet and outlet stream values of temperature, concentrations I, M, and R (in (kg mol)/m^3) and some dimensionless groups for the three runs of interest in the CFD curves in Figures 1 and 3, i.e., the run at the lowest and the highest temperature and at the temperature nearest the minimum. For discussion purposes, these runs will be referred to as the low-temperature, midpoint-temperature, and high-temperature runs. The outlet stream values are taken as representative of the bulk mean values. Jet temperature and concentrations in Table 2 correspond to the location of the maximum value of R in the jet for that run. The Damköhler numbers Da_{1I} and Da_{1R} are given for the jet conditions only. The dimensionless group KCL is the ratio of propagation rate to termination rate, i.e., $k_pM/k_{tc}R$ (also known as kinetic chain length). Columns 7 and 11 show the ratios of jet to outlet value R/R_{out} and KCL/KCL$_{out}$, respectively, for the total radical concentration R and KCL. Column 12 shows the similar ratio for the molar initiator consumption IC which can be defined as

$$\text{IC} = k_{tc}R/fk_pM = \text{moles of initiator consumed/mole of monomer polymerized}$$

Columns 13 and 14 show the values of the second Damköhler numbers Da_{2R} and Da_{2M} for the jet conditions. The significance of each entry in Table 2 will become clear in the following discussion.

The low-temperature run (250 ppm initiator; jet at 131 C; outlet at 146 °C) shows that Da_{1I} in the jet is much less than 1 (0.0003). Thus, in this case the initiator essentially leaves the jet unreacted. There can be no macrosegregation. Figure 5, which shows a K-sliced contour plot of total radical concentration for the low-temperature run, indicates clearly that radicals were made in the bulk and not in the jet in this run. The midpoint run (50 ppm; jet at 217 °C; outlet at 227 °C) has $Da_{1I} = 0.6$ and $Da_{1R} = 0.4$. Thus, no appreciable macrosegregation effects can be expected, and the reactor still behaves like a CSTR. In the high-temperature run (150 ppm; jet at 236 °C; outlet at 264 °C), the jet has a Da_{1I} of 2.3 and a Da_{1R} of 19.4. Thus, one can expect that in this case the initiator decomposes in the jet and the radicals that are produced undergo considerable termination in the jet due to macrosegregation indicated by the relatively high value of Da_{1R}. Figure 6, which is a K-sliced contour plot of total radical concentration for the high-temperature run, shows that in fact the maximum concentration of radicals occurred in the jet in this run indicating that appreciable amounts of radicals were made in the jet following initiator decomposition. Inspection of the initiator concentrations (column 4) shows that in this run, the outlet had no initiator implying that the initiator was essentially all consumed in the jet, a fact verified by a

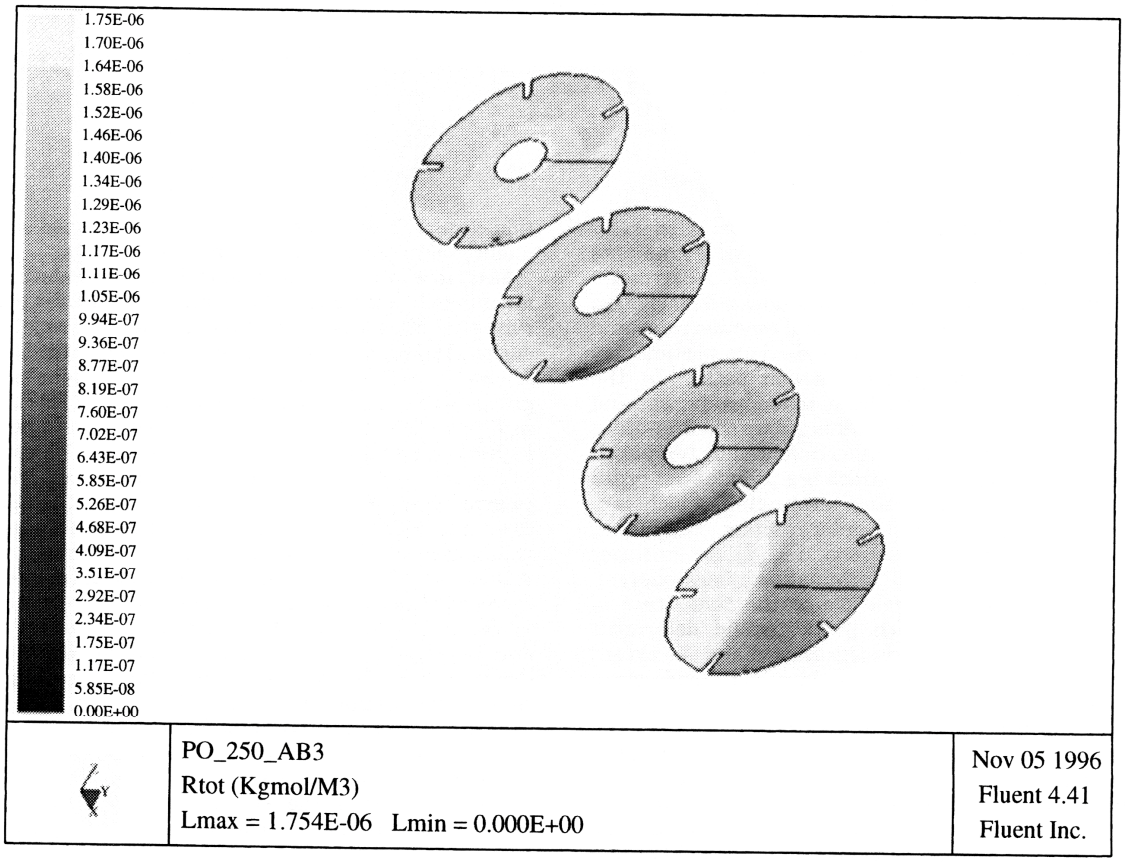

Figure 5. K-slice contours of R, total radical concentration, at K = 1, 21, 42, 62 for the low-temperature run for initiator A (250 ppm).

review of detailed CFD results. Inspection of the ratio R/R_{out} shows that there was indeed a very large gradient of radical concentration between the jet and the bulk at the high-temperature run evidenced by a ratio of 255 as opposed to 0.2 and 4.1 for the low- and midpoint-temperature runs, respectively. Inspection of the values of KCL ($k_pM/k_{to}R$) indicates that the ratio of propagation to termination rates in the jet decreases from 16 300 to 400 as one moves from the midpoint to the high-temperature indicating that macrosegregation in the jet was responsible for a drastic reduction in the ratio of propagation rate to termination rate which resulted in the observed increase in initiator concentrations necessary for sustaining temperatures beyond the minimum point in the CFD curve in Figure 1. As indicated above, KCL is also the kinetic chain length, and the figures of 16 300 and 400 represent a drastic drop in the average length of the dead polymer chains being made in the jet in the midpoint and the high-temperature runs, respectively. Furthermore, inspection of the ratio KCL/KCL_{out} shows the latter decreased from about 0.2 to 0.002 from the midpoint to the high-temperature indicating that chains that were being made in the jet were also very much shorter than the chains in the bulk in the high-temperature case than in the midpoint case. And finally inspection of the ratio IC/IC_{out} shows that the local relative initiator consumption increased from about 5.8 to 585 from the midpoint temperature to the high-temperature indicating that the macrosegregation in the jet was indeed responsible for the increase in initiator consumption in the CFD curve in Figure 3 mainly as a result of premature termination of short radical chains. It is important to point out here that the kinetic chain length values in this study are much higher than the actual kinetic chain values in real-life situations where chain transfer to monomer, dead polymer, solvent, etc., do occur. These reactions have been neglected in the present analysis for reasons given earlier. It is clear from the above comparisons that the macrosegregation effects that started past the midpoint temperature continually increased with temperature where at the high-temperature case the jet had considerable macrosegregation of radicals which terminated in the jet, a fact that can account for the departures from ideality observed in Figures 1 and 3.

Figure 7 shows temperature contours for the high-temperature run in Table 2 to provide the spatial distribution of temperature in this macrosegregated case. Note that macrogradients of temperature do exist around the jet. However, there are no very steep temperature gradients in or near the jet which provides support for the earlier arguments regarding the effects of temperature fluctuations on the scalar source terms.

Initiator B. Table 3 summarizes data relevant to macrosegregation effects for three selected CFD model runs for initiator B. Organization of Table 3 is identical to that of Table 2.

The low-temperature run (135 ppm initiator; jet at 132 °C; outlet at 148 °C) shows that Da_{1I} in the jet is again much less than 1 (0.003), which means that in this case also the initiator essentially leaves the jet unreacted and there can be no macrosegregation. The midpoint run (60 ppm; jet at 178 °C; outlet at 184 °C) has Da_{1I} = 0.1 and Da_{1R} = 1.5. Thus, still no macrosegregation effects can be expected, and the reactor still behaves like a CSTR. In the high-temperature run (135

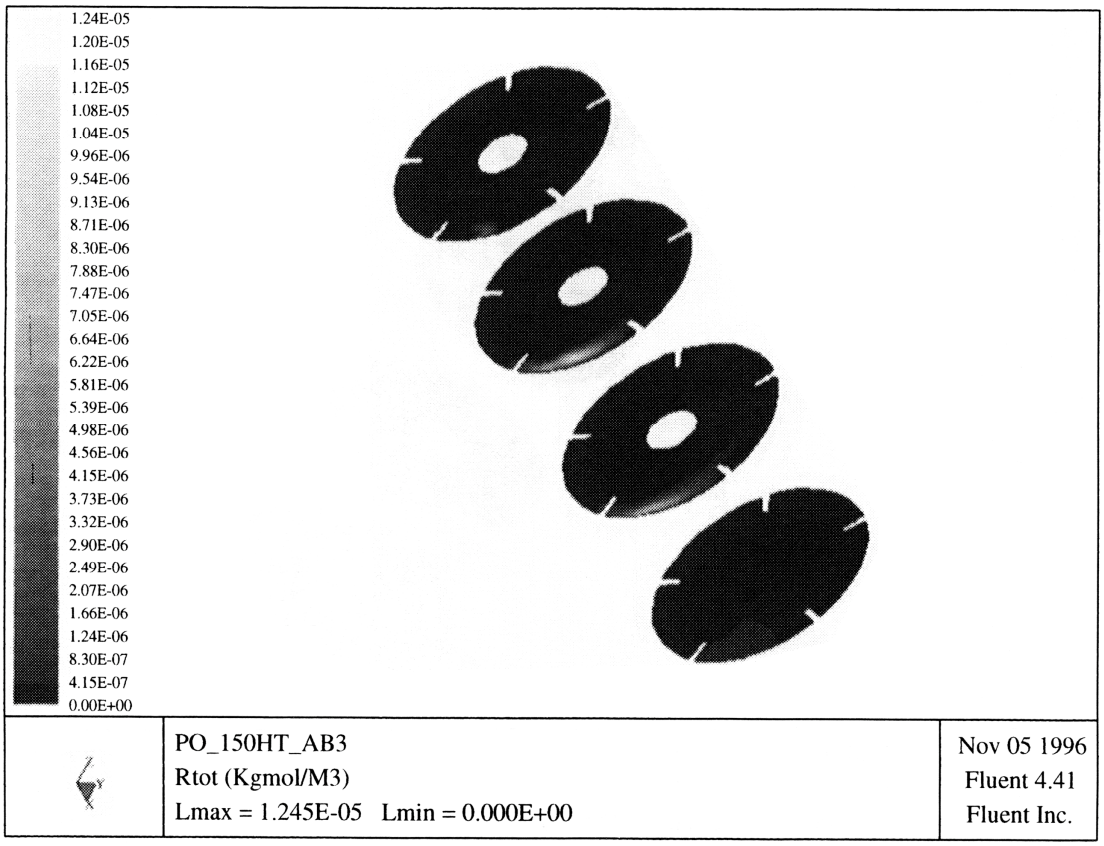

Figure 6. K-slice contours of R, total radical concentration, at $K = 1, 21, 42, 62$ for the high-temperature run for initiator A (150 ppm).

ppm; jet at 225 °C; outlet at 247 °C), the jet has a Da_{1I} of 2.0 and a Da_{1R} of 14.2. Thus, one can expect that in this case the initiator decomposes in the jet and the radicals that are produced undergo considerable termination in the jet due to macrosegregation indicated by the relatively high value of Da_{1R}. Inspection of the initiator concentrations (column 4) shows that in this run again, the outlet has no initiator implying that the initiator is probably all consumed in the jet, a fact verified by a review of detailed CFD results. Inspection of the ratio R/R_{out} shows that there was indeed a very large gradient of radical concentration between the jet and the bulk at the high-temperature run evidenced by a ratio of 169 as opposed to 0.3 and 5.2 for the low- and middle-point-temperature runs, respectively. Inspection of the values of KCL ($k_pM/k_{to}R$) indicates that the ratio of propagation to termination rates in the jet decreases from 2300 to 500 as one moves from the midpoint to the high-temperature indicating that macrosegregation in the jet was again responsible for a drastic reduction in the ratio of propagation rate to termination rate which resulted in the observed increase in initiator concentrations necessary for sustaining temperatures beyond the minimum point in the CFD curve in Figure 2. As indicated above, the figures of 2300 and 500 also represent a drastic drop in the average length of the dead polymer chains being made in the jet in the midpoint and the high-temperature runs, respectively. Inspection of the ratio KCL/KCL_{out} again shows that this ratio also decreased from about 0.1 to 0.0025 from the midpoint to the high-temperature case indicating that chains that were being made in the jet were very much shorter than the chains in the bulk in the high-temperature case than in the midpoint case. And finally inspection of the ratio IC/IC_{out} shows that the local relative initiator consumption increased from about 7.9 to 390 from the midpoint temperature to the high-temperature indicating that the macrosegregation in the jet was responsible for the increase in initiator consumption seen in the CFD curve in Figure 4 as a result of premature termination of short radical chains.

It can be concluded from the foregoing discussions that the macrosegregation effects that started past the midpoint temperature continually increased with temperature where at the high-temperature case the jet had considerable macrosegregation of radicals which terminated in the jet, a fact that can account for the departures from ideality observed in Figures 1–4.

Examination of the Microsegregation Closure. In order to reexamine the validity of the assumption that the fluctuation terms in eqs 13–15 can be dropped, the following reasoning can be followed: If in fact the homogenization of microscale concentration gradients by molecular diffusion occurred much faster than any reaction could take place, then the fluctuation terms in eqs 13–15 would actually be equal to zero. Therefore, the convection diffusion equation (eq 6) for the reactive scalars and the enthalpy balance equation would all have to be solved with source terms from eqs 12 and 17–19 which have only the time-mean values of the reactive scalars. Thus, the correct steady-state solution for each scalar and the temperature at any point in the grid would be equal to the time-mean value exactly. If one then calculated the values of the second Damköhler number $Da_{2R} = t_{DS}/t_c$ and $Da_{2M} = t_{DS}/t_p$, where $t_c = 1/k_{to}R$ and $t_p = \ln 2/(k_pR)$, at any point in the grid with the

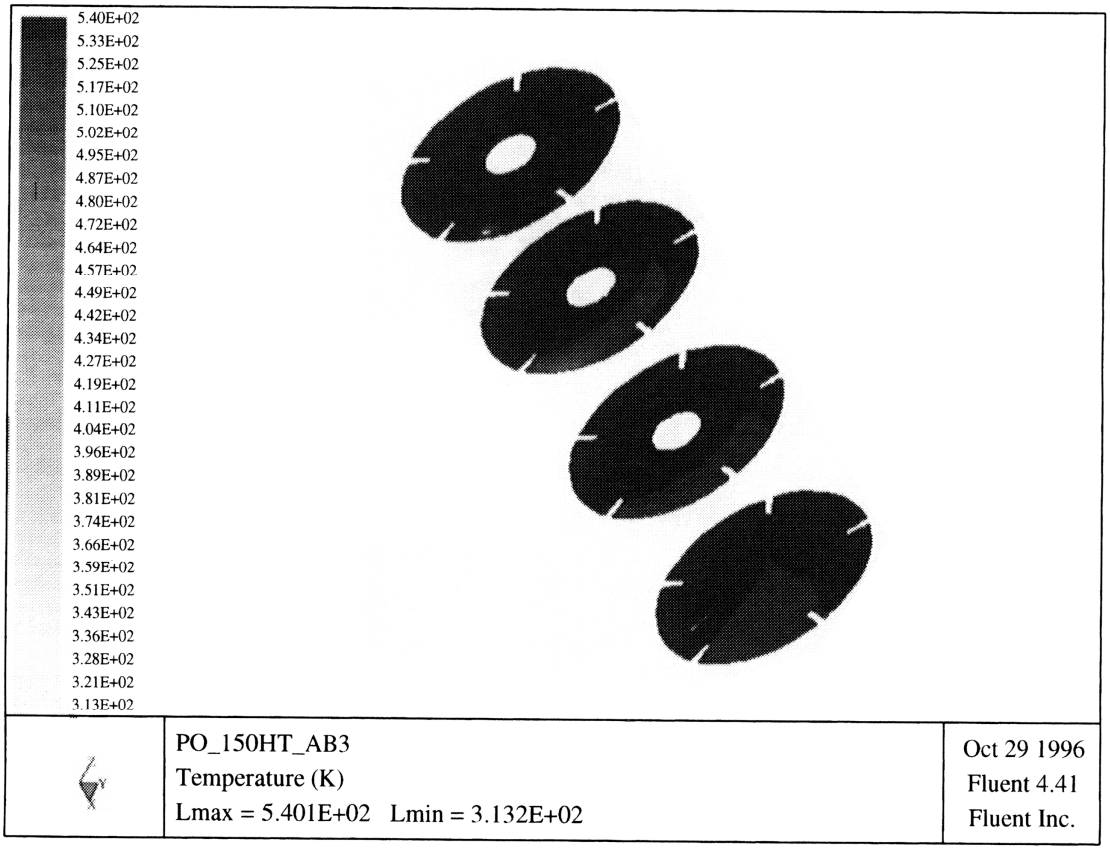

Figure 7. K-slice contours of temperature at $K = 1, 21, 42, 62$ for the high-temperature run for initiator A (150 ppm).

Table 3. Summary of Results for Selected CFD Runs with Initiator B

feed init (ppm)	value at	temp (°C)	$I \times 10^4$	M	$R \times 10^5$	R/R_{out}	Da_{1I}	Da_{1R}	KCL $\times 10^{-3}$	KCL/KCL$_{out}$	IC/IC$_{out}$	Da_{2R}	$Da_{2M} \times 10^{-3}$
135	jet	132	2.86	20.1	0.054	0.3	0.003	0.8	2.0	0.45	2.2	0.02	0.002
	outlet	148	0.63	18.7	0.16	1.0			4.4	1.00	1.0	0.05	0.03
60	jet	178	0.47	18.2	0.32	5.2	0.1	1.5	2.3	0.13	7.9	0.04	0.02
	outlet	184	0.006	17.3	0.062	1.0			18.2	1.0	1.0	0.02	0.02
135	jet	225	0.89	17.8	1.15	169	2.0	14.2	0.5	0.0025	390	0.3	0.16
	outlet	247	0.00	15.3	0.0068	1.0			195	1.0	1.0	0.005	0.006

exact (time-mean) values of R and the temperature one would find that these were smaller than unity (1.0). For if they were not, then the equations of the system would have had to include the covariance terms.

Columns 13 and 14 in Tables 2 and 3 show that the values of Da_{2R} and Da_{2M} calculated for the jet and the bulk with the time-mean values of R, and the temperatures (solved with the POM closure made here) are indeed much smaller than unity in all cases except in the high-temperature case in the jet where they are still appreciably smaller than unity with 0.5, 2.3×10^{-4}, and 0.3, 1.6×10^{-4} for Table 2 and Table 3, respectively. It is therefore concluded that the POM closure which consists of dropping the covariance terms in the source equations (eqs 13−15) and solving the system equations for the time-mean values results in a correct steady-state solution that satisfies all the boundary conditions of the system and the requirement that the second Damköhler numbers Da_{2R} and Da_{2M} be smaller than unity. Other steady-state solutions at much higher temperatures may exist, and they may require the inclusion of the covariance terms in eqs 13−15. However, these solutions would be beyond the temperature range of interest in the present study.

Conclusion

Although experimental data for commercial-scale reactors are not available for us to verify the results of the CFD model calculations, laboratory-scale data of Luft and Bitsch (1977), van der Molen *et al.* (1972, 1982), and Mercx *et al.* (1972) suggest that appreciable deviations from CSTR model predictions can be expected for commercial-scale reactors where the larger vessel dimensions render macrosegregation effects even more likely to occur. It has been shown that the CFD model does indeed predict significant differences from CSTR model predictions. Given the fact that the CFD model is based on mathematical descriptions of reacting scalar and energy balances (without adjusted parameters) in a 3-D flow field covering the entire reactor, it is tentatively concluded that commercial-scale LDPE vessel reactors can have significant macrosegregation effects past a critical steady-state adiabatic operating temperature that is specific to the initiator being used.

These nonidealities are responsible for the observed minima in the initiator consumption curves and the associated multiple steady states. The latter may be responsible for the fact that commercial reactors that are operated at a metastable state by closed-loop control are prone to easy temperature runaways and associated ethylene decomposition incidents. It is also concluded that microsegregation effects are essentially negligible in comparison to the macrosegregation effects in these reactors.

Nomenclature

C_A = concentration of A
C_B = concentration of B
I = concentration of initiator ((kg mol)/m^3)
M = concentration of monomer ((kg mol)/m^3)
R = total concentration of radicals ((kg mol)/m^3)
I_0 = concentration of initiator in feed
M_0 = concentration of monomer in feed
Q = feed flow rate
V = reactor volume (CSTR)
C_p = heat capacity
ΔH = heat of reaction
t_d = reaction time for initiator decomposition = ln $2/k_d$
t_c = reaction time for termination = $1/(k_{to}R)$
t_p = reaction time for propagation = ln $2/(k_pR)$
Sc = Schmidt number = ν/D
Pr = Prandtl number = γ/D
D = molecular diffusivity
k = kinetic energy of turbulence
ϵ = turbulent energy dissipation rate
ρ = density

Literature Cited

Baldyga, J.; Bourne, J. R. A Fluid Mechanical Approach to Turbulent Mixing and Chemical Reaction-Part II. Micromixing In The Light Of Turbulence Theory. *Chem. Eng. Commun.* **1984**, *28*, 243.

Baldyga, J.; Bourne, J. R. Simplification of Micromixing Calculations. I. Derivation and Application of New Model. *Chem. Eng. Res. Des.* **1989**, *42*, 83

Baldyga, J.; Bourne, J. R. Influence of Feed Pipe Diameter on Mesomixing in Stirred Tank Reactors. *Chem. Eng. Sci.* **1993**, *48*, 3383.

Bakker A.; Van den Akker, H. E. A. Single-Phase Flow in Stirred Reactors. *Chem. Eng. Res. Des.* **1994**, *72*, 573.

Buback, M. Free-Radical Polymerization up to High Conversion. A General Kinetic Treatment. *Makromol. Chem.* **1990**, *191*, 1575.

Chan, W.-M.; Gloor, P. E.; Hamielec, A. E. A Kinetic Model for Olefin Polymerization in High-Pressure Autoclave Reactors. *AIChE J.* **1993**, *39*, 111.

Crank, J. *The Mathematics of Diffusion*, second ed.; Clarendon Press: Oxford, 1975.

Fluent User's Guide, Version 4.3, Fluent, Inc., 1995.

Frankel, S. H.; Madnia, C. K.; Givi, P. Comparative Assessment of Closures for Turbulent Reacting Flows. *AIChE J.* **1993**, *39*, 899.

Hanks, M. L.; Toor, H, Relative Importance of Macro- and Micromixing in Turbulent Reacting Jets. *Ind. Eng. Chem. Res.* **1995**, *34*, 3252.

Kiparisssides, C.; Verros, G.; MacGregor, J. F. Mathematical Modeling, Optimization, and Quality Control of High-Pressure Ethylene Polymerization Reactors. *J. Macromol. Sci., Rev. Macromol. Chem. Phys.* **1993**, *C33* (4), 437.

Luft, G.; Bitsch, H. Effectiveness of Organic Peroxide Initiators in the High-Pressure Polymerization of Ethylene *J. Macromol. Sci., Chem.* **1977**, *A11* (6), 1089.

Marini, L.; Georgakis, C. Low-Density Polyethylene Vessel Reactors *AIChE J.* **1984**, *30*, 401.

Marini, L.; Georgakis, C. The Effect of Imperfect Mixing on Polymer Quality in Low Density Polyethylene Vessel Reactors. *Chem. Eng. Commun.* **1984**, *30*, 361.

Mercx, F. J.; van der Molen, Th. J.; de Steenwinkel, M. *Proceedings of the 5th European, 2nd International Symposium on Chemical Reaction Engineering*, Amsterdam, May 2–4, 1972; Elsevier: Amsterdam, 1972; Vol. B7, pp 41–48.

Ray, W. H. On the Mathematical Modeling of Polymerization Reactors *J. Macromol. Sci., Rev. Macromol. Chem.* **1972**, *C8*, 1.

Smit, L. The Use of Micromixing Calculations In LDPE Reactor Modelling. *4th International Workshop on Polymer Reaction Engineering*; Reichert, K. H., Moritz, H. U., Eds.; DECHEMA: Frankfurt, Germany, 1992; pp 77–92.

Stanford Research Institute, Polyethylene Overview, CEH Abstract, from http://www.sri.com/(1995).

Tennekes, H.; Lumley,L. J. *A First Course in Turbulence*; The MIT Press: Cambridge, MA, 1987.

Torvik, R.; Gravdahl, A. R.; Fredrikswn, G. R.; Meon, O.; Laurell, J. Design of HPPE Stirred Autoclaves Using 3D Computational Fluid Dynamics. *5th International Workshop on Polymer Reaction Engineering*; Reichert, K. H., Moritz, H. U., Eds.; DECHEMA: Frankfurt, Germany, 1995; pp 401–411.

van der Molen, Th. J.; van Heerden, C. The Effect of Imperfect Mixing on the Initiator Productivity in the High Pressure Radical Polymerization of Ethylene. *Adv. Chem. Ser.* **1972**, *109*, 92.

van der Molen, Th. J.; Koenen; Osterwijk, A. H.; van der Bend, H. Light-off Temperature and Consumption of 16 Initiators in LDPE Production. *Ing. Chim. Ital.* **1982**, *18*, 7.

Villermaux, J.; Pons, M.; Blavier, L. Comparison of Partial Segregation Models for The Determination of Kinetic Constants in a High Pressure Polyethylene Reactor. *ISCRE 8, The Eighth International Symposium on Chemical Reaction Engineering, Institution of Chemical Engineers Symposium Series*; **1984**; No. 87, pp 553–560.

Wang, M. H.; Calabrese, R. V.; Bakker, A. Effect of Reynolds No. on the Flow Generated by Pitched Blade and High Efficiency Turbines. Paper presented at Mixing XV, 15th Biennial North American Mixing Conference, June 18–23, 1995; Banff: Canada, 1995.

Zwietering, T. N. A Backmixing Model Describing Micromixing In Single-Phase Continuous Flow Systems. *Chem. Eng. Sci.* **1984**, *39*, 1765.

Received for review July 1, 1996
Revised manuscript received November 12, 1996
Accepted November 13, 1996[⊗]

IE960374U

[⊗] Abstract published in *Advance ACS Abstracts,* January 1, 1997.